

MEASUREMENT OF HELIUM GENERATION IN AISI 304 REFLECTOR AND BLANKET ASSEMBLIES AFTER LONG-TERM IRRADIATION IN EBR-II—F. A. Garner, B. M. Oliver, L. R. Greenwood (Pacific Northwest National Laboratory),¹ D. L. Porter (Idaho National Laboratory), and T. Allen (University of Wisconsin)

OBJECTIVE

The object of this effort is to determine whether potential variations in He/dpa ratio participated significantly in development of void swelling in a data base on AISI 304 stainless steel where relatively large variations in dpa rate were thought to primarily determine the duration of the transient regime of swelling.

SUMMARY

Five hexagonal ducts constructed from AISI 304 stainless steel in the annealed state were removed from rows 8-14 of the EBR-II fast reactor after many years of irradiation to study the effect of atomic displacement rate on void swelling. For this objective it was important to ensure that the observed differences in void swelling were not strongly influenced by variations in helium/dpa ratio. The two major contributions to helium production arise from the nickel and boron content of the steel. However, the boron content was unspecified and therefore unknown, but it was determined from an unirradiated archive duct by converting a well-defined fraction to helium and then measuring the helium content using isotopic dilution mass spectrometry. The same technique was used to measure the total helium in the irradiated duct specimens. After separating the boron contribution from the total measured helium it was possible to determine the contribution from various fast and thermal neutron interactions with the other major elements in the steel and compare the helium generation with predicted values. One important conclusion of the study is that the range of He/dpa ratios over the five subassemblies was not very large, allowing the observed changes in swelling to be attributed primarily to variations in displacement rate and temperature.

PROGRESS AND STATUS

Introduction

Far from the active core regions of a small fast reactor it becomes somewhat more difficult to calculate the helium generation in stainless steel components of the reflector and blanket regions. This is particularly true for components that served many years in EBR-II while the core and reflector regions underwent many modifications, or for components which were moved and sometimes rotated during their lifetime.

In an experiment directed toward determination of the effect of displacement rate on void swelling of annealed AISI 304 stainless steel, it was important to ensure that observed differences in void swelling were primarily in response to displacement rate and not other important variables such as the helium/dpa ratio that might exhibit time-dependent or position-dependent variations [1-3]. Helium is well known to accelerate the nucleation of voids and shorten the transient regime of swelling. However, since there are helium sources associated with both low energy and high energy neutrons, one can not confidently assume that lower flux regions with their inherently softer spectra will lead to consistent decreases or increases in helium generation per dpa. As the high energy source of helium declines the low energy source tends to increase and the net change can move in either direction.

¹Pacific Northwest National Laboratory (PNNL) is operated for the U.S. Department of Energy by Battelle Memorial Institute under contract DE-AC06-76RLO-1830.

Rather than relying only on calculations of expected helium content for such complicated histories, the helium content was measured directly using an isotopic dilution mass spectrometry method known to be very accurate. Since some significant fraction of the helium in these relatively soft spectral regions arises from transmutation of boron it was necessary to determine the unknown boron content using an archive duct of the same heat of steel.

Experimental Details

The width of the face of these hexagonal ducts is 2.9 cm and the duct is 1 mm thick. Four of the five ducts employed in this study were constructed from the same heat of steel designated 772864 and were irradiated for the majority of their lifetime in rows 8, 9, and 10 of EBR-II, as schematically shown in Fig. 1. The two ducts that were irradiated in row 10 were on opposite sides of the core. The fifth duct was much older and spent most of its residence time in Row 14 but was constructed from an earlier different heat of steel prepared to the same specification but without an available archive, but analyses conducted after irradiation showed that the composition of the two heats was quite similar, as shown in Table 1.

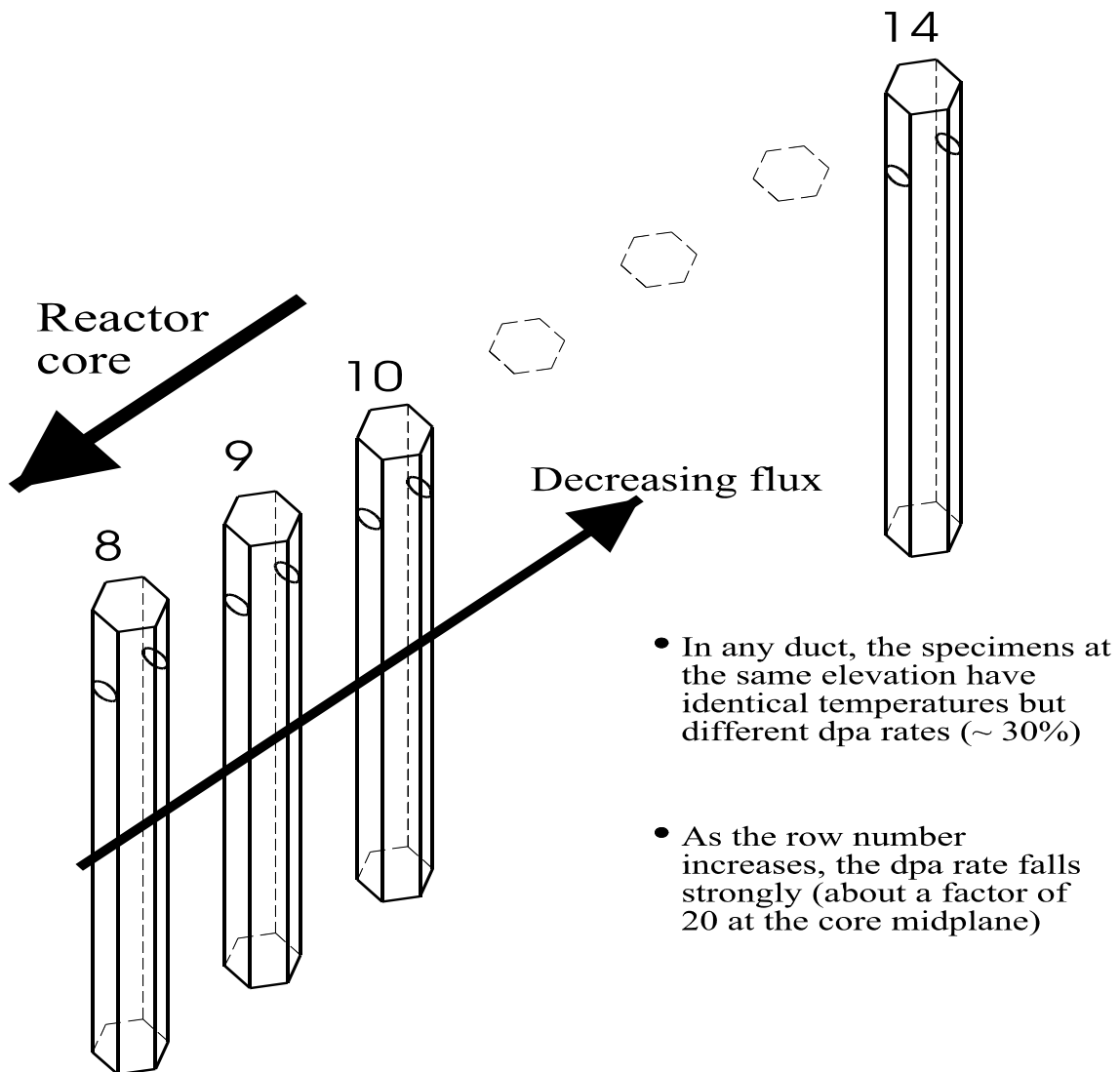


Fig. 1. Schematic representation of flux-effects experiment in EBR-II.

Table 1. Composition of heat 772864 in wt%

	N₂	Mn	Cr	Ni	Co	Cu	Si	Mo	Nb	P	C	S
Vendor Specification for Row 14 duct	----	0.8	18.56	9.05	----	----	0.51	----	----	0.027	0.07	0.003
Measurements at EBR-II on other ducts	0.05	0.832	----	8.20	0.016	0.02	----	0.011	0.001	----	----	----

---- = not specified or measured

As shown in Table 2 and also Fig. 2 these ducts remained in the reflector and blanket regions of EBR-II for different periods spanning many years, with only the two row 10 ducts remaining in the same position and orientation throughout their residence. However, while the row 10 ducts (U9007 and U9009 at 32 and 27 dpa, respectively) were not moved, the core, reflector and blanket regions underwent many significant modifications during this period. During the Liquid Metal Reactor Program the core was expanded to include many lower worth assemblies, with many changes made from run-to-run.

Table 2. Run history and temperature assignments

Assembly	EBR-II Row	MWD in this Row*	Time Fraction	dpa (max)	Temperature Assignment**
U9007	10	187,505	1.00	32.0	average
U9009	10	184,463	1.00	27.0	average
U8972	9	91,166	0.41	33.0	time average in row 9 only
	15	133,785	0.59	1.4	
U9807	8	60,165	0.36	32.0	time average in row 8 only
	16	107,495	0.64	0.9	
U1603	8	5,951	0.02	2.4	time average in row 14 only
	14	348,584	0.98	7.6	

*MWD = megawatt-days

**Temperatures are not relevant to helium production or retention. See references 1 and 3 for details.

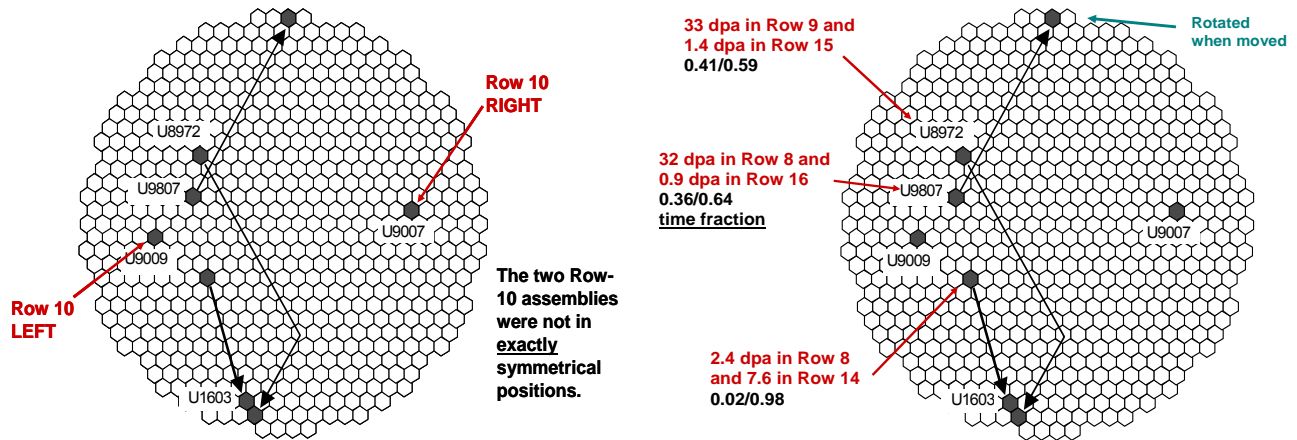


Fig. 2. Schematic representation of assembly location and dose history.

Twenty 2.0 cm diameter specimens spanning a large axial range about the core center-plane were removed from each of the inboard and outboard faces of each duct. The faces examined were defined by the orientation and row where the majority of the dose was accumulated, with inboard-outboard defined relative to the core centerline to maximize the dose difference. The average density of each 2.0 cm disk was measured using an immersion density technique and the results are reported elsewhere [1-3]. After density measurements were completed, smaller specimens averaging ranging from ~2 to ~4 mg were produced from five of the twenty disks from each of the inboard and outboard sides of each duct and used for determination of helium content. A total of 40 specimens were measured, taken from two opposing flats of each assembly.

The time-averaged values of temperature and dpa relevant to each duct and individual specimen were determined at the EBR-II facility of Argonne National Laboratory. These calculations are reported in [3] and the dpa and methods of temperature assignments are shown in Table 2.

An archive duct of the production heat used for ducts in rows 8-10 was obtained and a ~30 mg sample was cut from one of the faces of the duct. For the helium analyses, specimens were prepared from each supplied sample by sectioning using small diagonal cutters. Before each use, the cutters were cleaned by wiping several times with a dry paper wipe. Prior to analysis, each specimen was cleaned in acetone and air-dried. The mass of each specimen was then determined using a calibrated microbalance traceable to the National Institute of Standards and Technology (NIST). Mass uncertainty is estimated to be ± 0.002 mg. Sample etching to remove at least 0.013 mm was performed to remove sufficient material to avoid errors associated with α -recoil across specimen surfaces, or surface contamination. Two separate measurements were made on specimens cut from each sample.

Helium analyses were conducted using isotope-dilution gas mass spectrometry following vaporization in a resistance-heated tungsten-wire crucible in one of the helium mass spectrometer system's high-temperature vacuum furnaces [4]. The absolute amount of ^4He released was measured relative to a known quantity of added ^3He "spike." Each helium spike was obtained by expanding and partitioning a known quantity of gas through a succession of calibrated volumes [5]. Additionally, the mass spectrometer was calibrated for mass sensitivity during each series of runs by analyzing known mixtures of ^3He and ^4He .

The results of the gas analyses are presented in Figs. 3 and 4 as gas concentrations in atomic parts per million (10^6 atom fraction). Conversion from total gas atoms released to gas concentration was based on a calculated value of 1.097×10^{22} atoms/gram for the 304 stainless steel material. It should be noted, however, that this conversion value, and the gas concentrations obtained using it, are not very sensitive to small changes in material composition. Uncertainty in the individual helium analysis results,

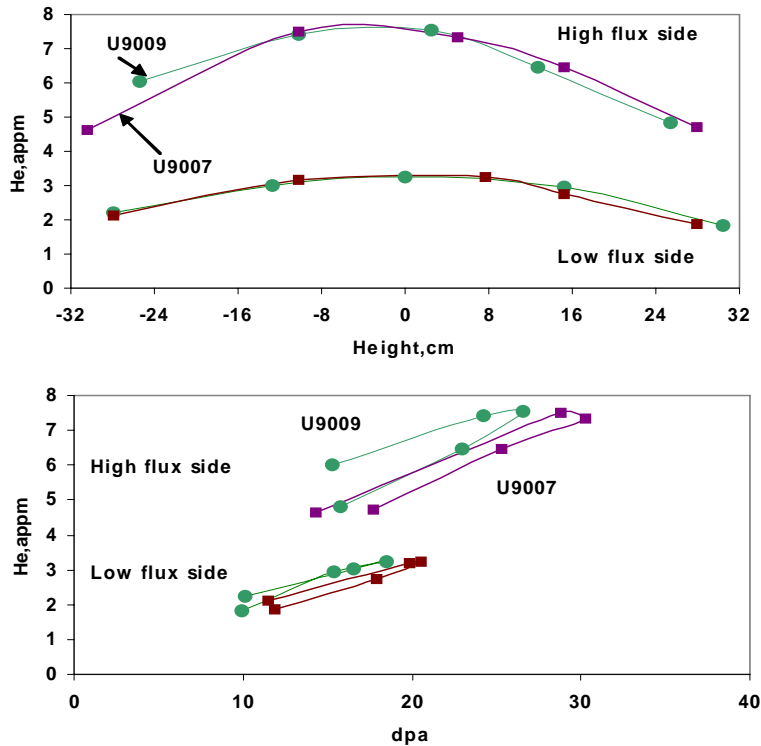


Fig. 3. Helium measurements of the two row 10 assemblies vs. axial location and dpa level. Note the very clear separation in generation rate between the low and high flux sides.

determined from the cumulative uncertainties in the sample mass, the isotope ratio measurement, and the spike size, is estimated to be ~1%.

The boron content in the hex-can sample was determined using a method similar to neutron activation. The sample was exposed to a known dose of thermal neutrons in order to convert a known fraction of the ^{10}B isotope to helium via the $^{10}\text{B}(n,\alpha)^7\text{Li}$ reaction. After irradiation, the helium generated was measured in several smaller specimens (~3.5 mg) cut from the sample, and used to determine the boron content, assuming an isotopic abundance of 19.9% for ^{10}B . Neutron dosimetry samples, in the form of a well characterized Al- ^6Li alloy wire, were included in the irradiation assembly to accurately determine the thermal neutron fluence via the $^6\text{Li}(n,\alpha)^3\text{H}$ reaction. The thermal neutron cross sections for the ^{10}B and ^6Li samples are well known.

The irradiation of the archive specimens was conducted in the research reactor at McMaster University in Canada. The irradiation time and thermal fluence were 160 hours and 2.04×10^{19} n/cm², respectively. The thermal-to-fast neutron ratio in this spectrum was approximately six, ensuring that >99% of the helium was generated from the boron with no significant amount of helium generated from the major elements, Ni, Fe, Cr, etc.

Results and Discussion

As discussed in references 1 and 2 there was a very clear and consistent effect of flux on void swelling in AISI 304 stainless steel at every temperature studied, providing that some other unrecognized variable did not contribute strongly. For void swelling the helium generation rate is known to often be a strong

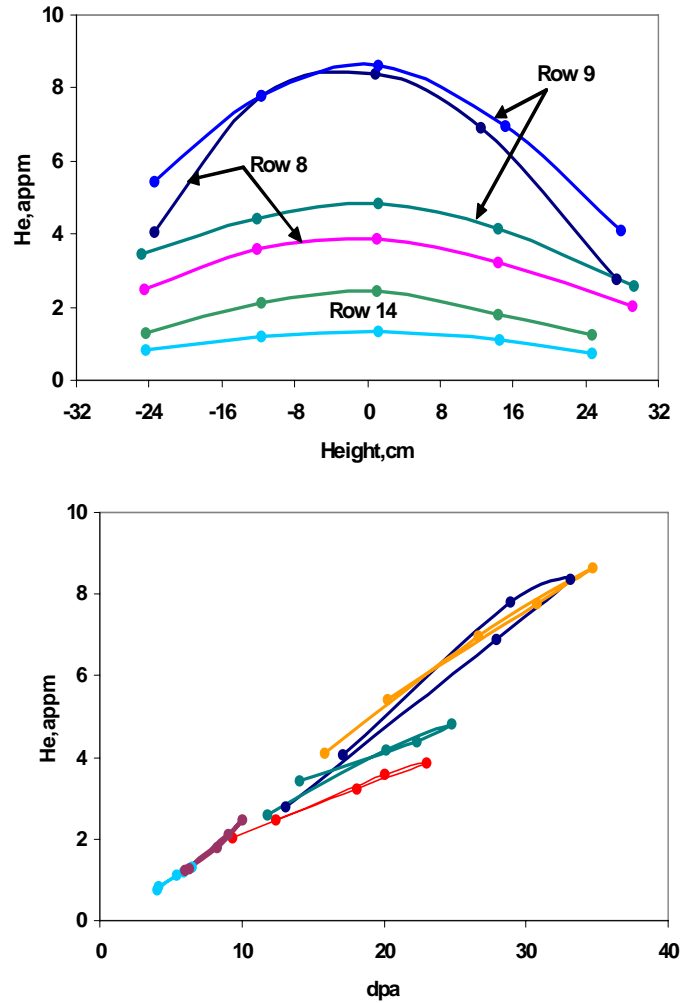


Fig. 4. Helium measurements on assemblies in rows 8, 9, and 14 vs. axial location and dpa level. Higher levels of helium are reached on the inboard face compared to the outboard face.

contributor to the onset of swelling, especially when the steel initially resists swelling [6]. While annealed 304 stainless steel is known not to be very resistant to swelling [6,7], it was prudent to check the possibility that the helium/dpa generation rate might be varying strongly. After measuring the total helium content the first step in assessing its origin lies in the determination of the boron content. The natural boron content in the archive samples was determined in this study to be 1.4 wt. ppm, corresponding to 0.25 wt. ppm ^{10}B , or 1.4 appm ^{10}B) with an uncertainty calculated to be about $\pm 3\%$. Therefore, even at complete burnup the maximum helium arising from the ^{10}B source could not exceed 1.4 appm. Most measured helium levels are significantly larger, at minimum a factor of ~ 2 higher, indicating that the primary helium contributions at higher exposures came from Ni, Fe and Cr.

The results of the helium measurements on the irradiated specimens are shown vs. both position and vs. dpa in Figs. 3 and 4. Note that the two row 10 assemblies have remarkably similar profiles even though the total exposures of the two assemblies are $\sim 16\%$ different. The helium generation rate per dpa on the high flux side of the row 10 assemblies is measurably larger than that of the low flux sides. There is also some small variation in total helium generation between the upper and lower portions of the row 10

assemblies with slightly more helium produced in the lower portion of the assembly. This difference is not so pronounced in the other assemblies and may reflect some influence of their movement during residence. For all subassemblies, however, the He/dpa ratio is relatively independent of axial location as shown in Fig. 5.

When all He concentration data are plotted vs. dpa, it is seen in Fig. 6 that the helium generation rate averages about ~ 0.25 appm/dpa. While some assemblies lie above or below this average rate, the variations are not large enough or systematic enough to significantly impact the conclusion of a strong dependence of dpa rate on swelling. Together with the finding that the total helium concentration never exceeds 10 appm this allows us to conclude that the range of He/dpa ratios over the five subassemblies is not very large, allowing the observed changes in swelling to be attributed primarily to variations in displacement rate and temperature, with helium playing at most a second-order role.

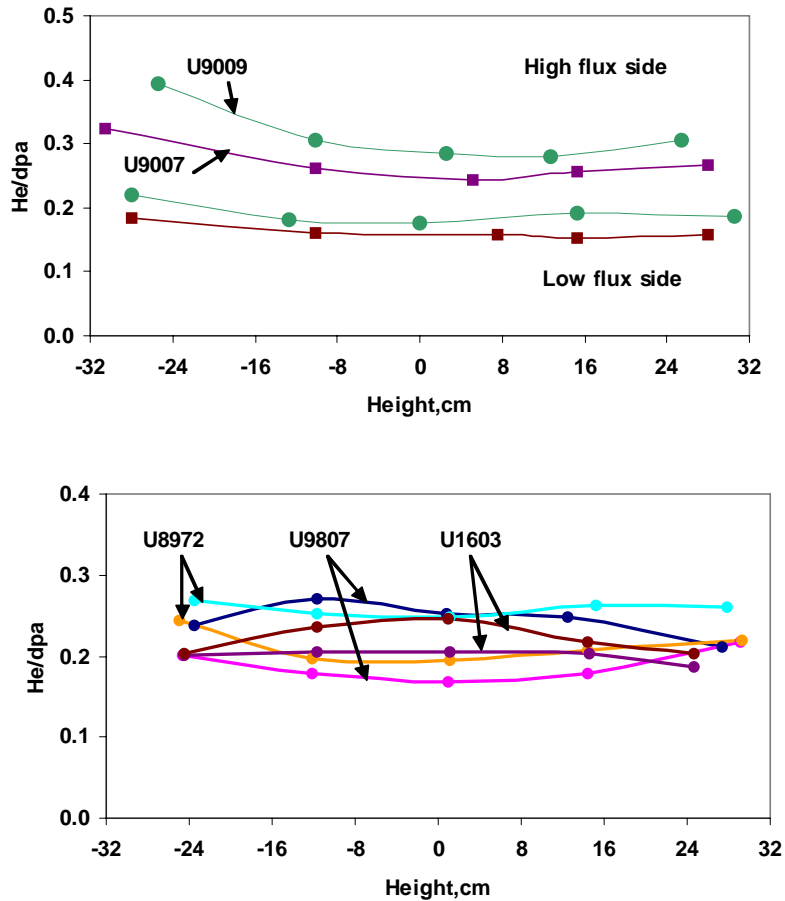


Fig. 5. Helium/dpa ratios of assemblies in row 10 (top) and rows 8, 9 and 14 (bottom) vs. axial location.

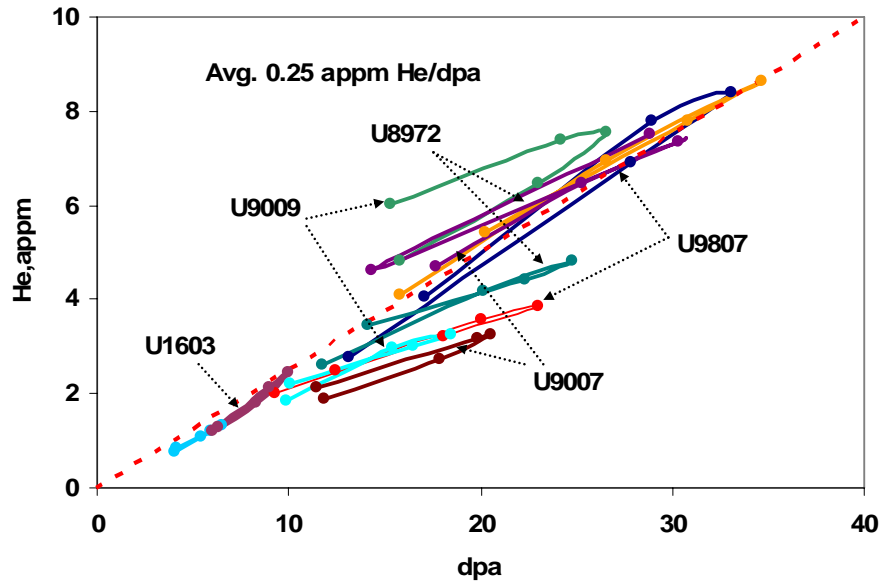


Fig. 6. Compilation of helium measurements for all assemblies vs. dpa level, showing an average generation rate of ~ 0.25 appm/dpa.

When the components have experienced a complicated history in neutron flux-spectra the need for measurements of time-integrated helium generation can be demonstrated using calculated flux-spectra that were available early in the life of EBR-II. Detailed flux-spectra derived from the EBR-II reactor low power dosimetry run designated 78C were available for comparison [8] and the total integrated time were used to make comparisons between 78C-based calculations and our measurements. However, the core has undergone numerous changes in local experimental loading over the lifetime of these assemblies. With exception of U1603 (in the core from run 25 to 170), all assemblies were put into reactor during runs 95-118, and stayed through runs 166-170. During the lifetime of these assemblies EBR-II underwent significant expansion to accommodate a growing number of experimental subassemblies. This expansion tended to reduce the local neutron flux over time.

As shown in Fig. 7 the 78C-based predictions of dpa are indeed significantly larger than those calculated for the mid-point of the assemblies, with the magnitude of over-prediction increasing strongly at lower row numbers. Note that significantly more helium was measured in row 10 than was predicted. Figure 8 shows that the predicted helium for row 8 is also significantly lower than measured in row 8, but also for rows 9 and 14.

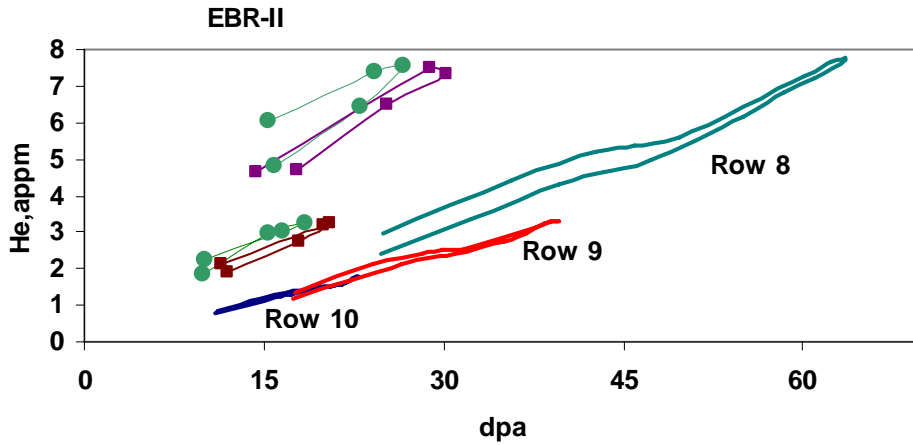


Fig. 7. Comparison of measured values of helium for the two row 10 assemblies vs. predicted values (calculated at assembly center) for rows 8, 9 and 10. Note that the measured values of helium for row 10 assemblies are significantly larger than predicted.

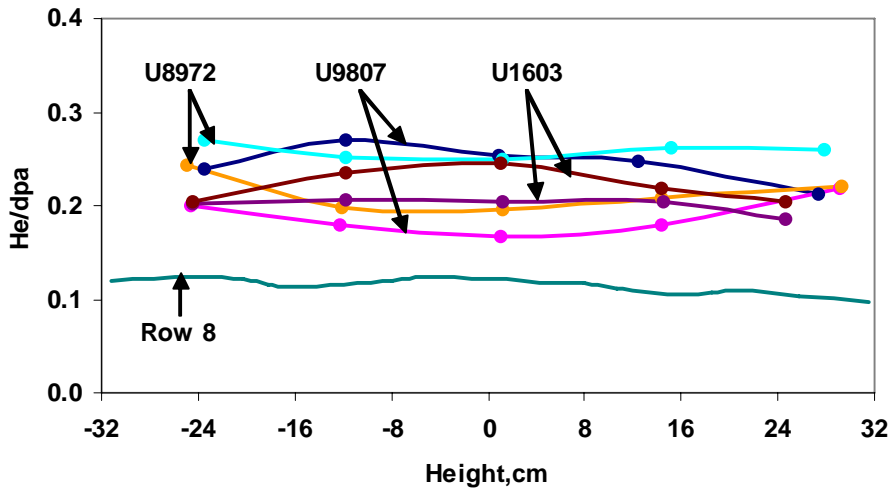


Fig. 8. Comparison of measured values of helium/dpa vs. axial location for assemblies in rows 8, 9 and 14 vs. prediction for Row 8. Note that significantly more helium is generated in row 8 than was predicted.

This apparently contradictory set of conclusions is a reflection of the fact that helium is generated primarily by nickel in a Fe-Cr-Ni alloy, but there are two competing reactions [9-14]. The first helium contribution arises from a high-energy reaction (n, α) with threshold energy of ~ 1 MeV. As the core expanded the average neutron flux and energy both tended to decrease in the reflector region. On the other hand the low-energy two-step $^{58}\text{Ni}(n, \gamma)^{59}\text{Ni}(n, \alpha)^{56}\text{Fe}$ reaction sequence increases in importance in softer spectra and dominates the helium production in this experiment. In addition the $^{10}\text{B}(n, \alpha)^7\text{Li}$ reaction also becomes more important in softer spectra.

These Run 78C predictions confirm two aspects of the measured behavior. First, Fig. 7 shows that there is indeed a tendency for slightly higher helium generation rates in the lower portion of the core compared

to the upper portion. Second, Fig. 8 shows that the He/dpa rate is relatively constant along the axial direction of a given assembly, both in agreement with the results of the current study.

Conclusions

The helium generated in AISI 304 stainless steel during irradiation in the EBR-II fast reactor is a sensitive function of neutron flux-spectra. When the flux-spectra vary over the residence time of a long-lived component it becomes more difficult to predict the accumulated helium, especially when the time history of the component is complicated and when the components reside in the blanket and reflector regions of the reactor.

In such cases the helium is best measured using techniques such as isotope-dilution gas mass spectrometry. If it is desirable to predict the relative contributions of high-energy (n, α), low energy ^{58}Ni (n, γ) ^{59}Ni (n, α) ^{56}Fe and low energy ^{10}B (n, α) ^7Li reactions, then the detailed composition of the steel must be known. When the boron concentration has not been measured then the ^{10}B (n, α) ^7Li reaction can be used with archive material to determine its concentration and contribution to helium production. In a complicated time-history experiment where it was important to know the relative roles of He/dpa ratio and dpa rate, it was demonstrated in this report that the He/dpa ratio did not vary strongly among the experimental samples and was most likely only a variable of second-order importance compared to the effect of dpa rate on void swelling of AISI 304 stainless steel.

References

- [1] G. M. Bond, B. H. Sencer, F. A. Garner, M. L. Hamilton, T. R. Allen, and D. L. Porter, Void Swelling of Annealed 304 Stainless Steel at ~370-385 °C and PWR-Relevant Displacement Rates, 9th International Conference on Environmental Degradation of Materials in Nuclear Power Systems—Water Reactors, 1999, 1045–1050.
- [2] F. A. Garner, D. J. Edwards, S. M. Bruemmer, S. I. Porollo, Yu. V. Konobeev, V. S. Neustroev, V. K. Shamardin, and A. V. Kozlov, Recent Developments Concerning Potential Void Swelling of PWR Internals Constructed from Austenitic Stainless Steels, Proceedings of Fontevraud 5, Contribution of Materials Investigation to the Resolution of Problems Encountered in Pressurized Water Reactors, September 23–27, 2002, paper #22, on CD.
- [3] F. A. Garner, M. L. Hamilton, D. L. Porter, T. R. Allen, T. Tsutsui, M. Nakajima, T. Kido, T. Ishii, Determination of Damage Rate Dependence of Void Swelling of Solution-Annealed 304 Stainless Steel Using Irradiated EBR-II Reflectors (in preparation).
- [4] B. M. Oliver and H. Farrar, Mass Spectrometer System to Determine Very Low Levels of Helium in Small Solid and Liquid Samples, J. Vacuum Sci. Technol. A4 (1986) 1740.
- [5] B. M. Oliver, J. G. Bradley, and H. Farrar, Helium Concentration in the Earth's Lower Atmosphere, Geochimica Cosmochimica Acta 48 (1984) 1759.
- [6] F. A. Garner, Chapter 6: Irradiation Performance of Cladding and Structural Steels in Liquid Metal Reactors, Materials Science and Technology: A Comprehensive Treatment, Vol. 10A Nuclear Materials, B. R. T. Frost (ed.), VCH Publishers, 1994, 419–543.
- [7] F. A. Garner and D. L. Porter, A Reassessment of the Swelling Behavior of AISI 304L Stainless Steel, International Conference on Dimensional Stability and Mechanical Behavior of Irradiated Metals and Alloys, Brighton, England, 1983, 41–44.
- [8] F. C. Franklin, E. R. Ebersole, and R. R. Heinrich, Analysis of EBR-II Low-Power Dosimetry Run 78C, Argonne National Laboratory Report, Vol. ANL-77-76, 1977.
- [9] L. R. Greenwood, F. A. Garner, and B. M. Oliver, Helium Generation Rates in Isotopically Tailored Fe-Cr-Ni Alloys Irradiated in FFTF/MOTA, J. Nucl. Mater. 191–194 (1992) 1051–1055.
- [10] F. A. Garner, L. R. Greenwood, and D. L. Harrod, Potential High Fluence Response of Pressure Vessel Internals Constructed from Austenitic Stainless Steels, Sixth International Symposium on Environmental Degradation of Materials in Nuclear Power Systems—Water Reactors, San Diego, Calif., 1993, 783–790.
- [11] L. R. Greenwood, F. A. Garner, and B. M. Oliver, An Assessment of the Ni-59 Isotopic Tailoring

Technique to Study the Influence of Helium/dpa Ratio, *J. Nucl. Mater.* 212–215 (1994) 492–497.

[12] F. A. Garner, L. R. Greenwood, and B. M. Oliver, A Reevaluation of Helium/dpa and Hydrogen/dpa Ratios for Fast Reactor and Thermal Reactor Data Used in Fission-Fusion Correlations, ASTM STP 1325, *Effects of Radiation on Materials: 18th International Symposium*, American Society of Testing and Materials, R. K. Nanstad, M. L. Hamilton, F. A. Garner, and A. S. Kumar (eds.), 1999, 794–807.

[13] F. A. Garner, B. M. Oliver, and L. R. Greenwood, The Dependence of Helium Generation Rate on Nickel Content of Fe-Cr-Ni Alloys Irradiated at High dpa Levels in Fast Reactors, *J. Nucl. Mater.* 258–263 (1998) 1740–1744.

[14] F. A. Garner and L. R. Greenwood, Survey of Recent Developments Concerning the Understanding of Radiation Effects on Stainless Steels Used in the LWR Power Industry, 10th International Conference on Environmental Degradation of Materials in Nuclear Power Systems—Water Reactors, 2003, 887–909.